Advances in Clathrate Research

Anders Bentien, Wilder Carrillo-Cabrera, Michael Baenitz, Michael Baitinger, Horst Borrmann, Sergei Budnyk, Roman Demchyna, Vladimir A. Ivanshin [1], Kirill Kovnir, Ulrike Köhler, Silke Paschen [2], Yurii Prots, Walter Schnelle, Ulrich Schwarz, Jörg Sichelschmidt, Peter Thalmeier, Vladimir Voevodin, Alexander Yaresko [3], Huiqiu Yuan [4], Ivica Zerec, Yuri Grin, and Frank Steglich

Introduction

In our previous scientific institute reports research results on clathrates have been presented [1,2]. This topic constitutes a main field of collaboration between the chemistry and physics research fields. As far as publications and the scientific output are concerned, our collaboration has been productive and resulted in four dissertations [3–6]. Our goal is to search for new rare earth containing Kondo insulators among clathrates. The fundamental idea is to combine the power factor ($S^2\sigma$, S is the thermopower and σ the electrical conductivity), which typically is large well below room temperature, of Kondo insulators with the low thermal conductivity (κ) of a cage-structured compound, such as the clathrates, to obtain a material with superior thermoelectric cooling properties, i.e. a large $ZT = S^2\sigma/\kappa$. Starting from the divalent non-magnetic reference compound $Ba_8Ga_{16}Ge_{30}$, the Ba–Ga–Ge system was investigated which led to the discovery of Ba_6Ge_{25}.

Structural phase transition in Ba_6Ge_{25}

The crystal structure and part of the exotic physical properties of the new Ba_6Ge_{25} clathrate have been discussed in previous scientific reports [1, 2]. Its exotic properties are a consequence of a two-step first-order phase transition at about T_{S1}/T_{S2} (down) $\approx$ 230 K / 180 K during cooling and at T_{S2}/T_{S1} (up) $\approx$ 190 K / 230 K during heating. Preliminary X-ray powder diffraction study [1] revealed a two-step anomalous volume increase by cooling through the phase transition. The major structural change involved was the displacement of two crystallographically different Ba atoms (Ba2 and Ba3). However, due to the resolution of the method, structural variations of the Ge framework are not conclusive. Therefore, Ba_6Ge_{25} has been studied by single-crystal X-ray diffraction methods in the temperature range 95 K to 300 K [7].

At room temperature, the cubic Ba_6Ge_{25} structure (space group $P4_132$) is characterized by three crystallographic barium sites (Ba1, Ba2, Ba3) and six germanium sites (Ge1, Ge2, Ge3, Ge4, Ge5, Ge6). The crystal structure consists of a non-space filling 3D arrangement of condensed pentagonal dodecahedra Ge_{20} with Ba1 inside the cages (Ba1@Ge_{20}), generating a zeolite-like channel. The Ba2 and Ba3 atoms occupy positions in the channel. Per Ba_6Ge_{25} formula unit, 8 out of 25 germanium atoms are three-bonded (3b), each of them accommodating a lone-pair and acting as charge acceptor. According to the Zintl–Klemm concept [8, 9] they are considered (3b)Ge^- ions. The Ba atoms are electron donors, i.e. 12 electrons per formula unit are donated to the germanium framework. Since the remaining 17 Ge atoms are four-bonded (4b) neutral species, the Zintl electron counting rule results in four excess electrons (4 e^-) per formula unit.

Twenty-six single-crystal X-ray diffraction data sets were recorded in the temperature range 95 K – 295 K and confirm that the space group symmetry of Ba_6Ge_{25} remains unchanged within this temperature interval, in agreement with the previous powder X-ray diffraction study (T = 10 K – 295 K). A close inspection of the difference electron-density maps around the Ba atoms reveals a distinct deformation, in the crystal structure, as function of temperature. This is illustrated in Fig. 1. In order to have comparable parameters in the entire temperature range, we used split atom positions to describe the distorted electron densities. Ba1, Ba2 and Ba3 are described with a one, two or three split atom site, depending on the point symmetry. The most interesting feature, below 225 K ($\approx T_{S1}$(down)), is the appearance of a second split atom site, Ba2‴, in the vicinity of the Ba2 site (described by Ba2′ and Ba2″ at $T > 220$ K). This defines step *S1* of the phase transformation. The densities at Ba1 and Ba2 start to deform slightly at 225 K, but below 180 K the deformation has increased rapidly, defining step *S*2 of the transformation. Below T_{S2}(down) $\approx$ 180 K, the changes in the electron density for all Ba sites are relatively small.

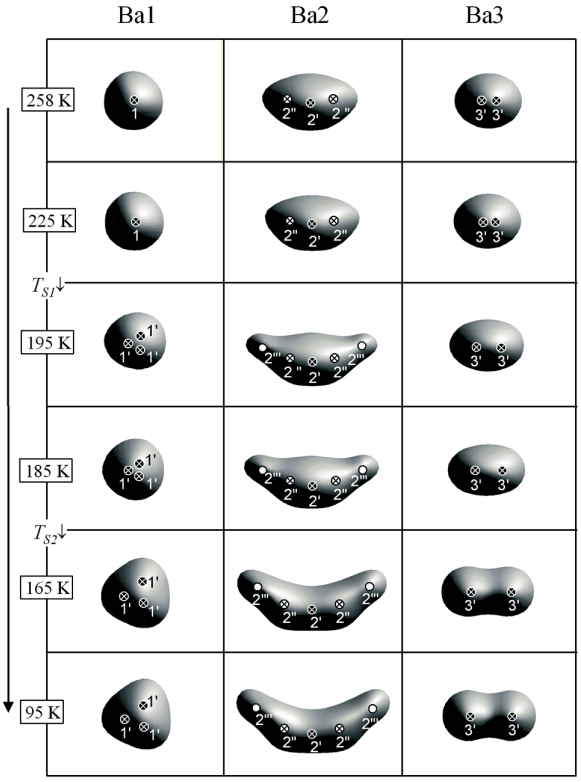

Fig. 1: Difference electron-density (isosurfaces at 11 e/Å^3) at Ba1 (left), Ba2 (middle) and Ba3 (right) sites in Ba_6Ge_{25} as a function of temperature (cooling sweep). The split atom sites which have been used to describe the electron density distribution are marked in the range by appropriate labels.

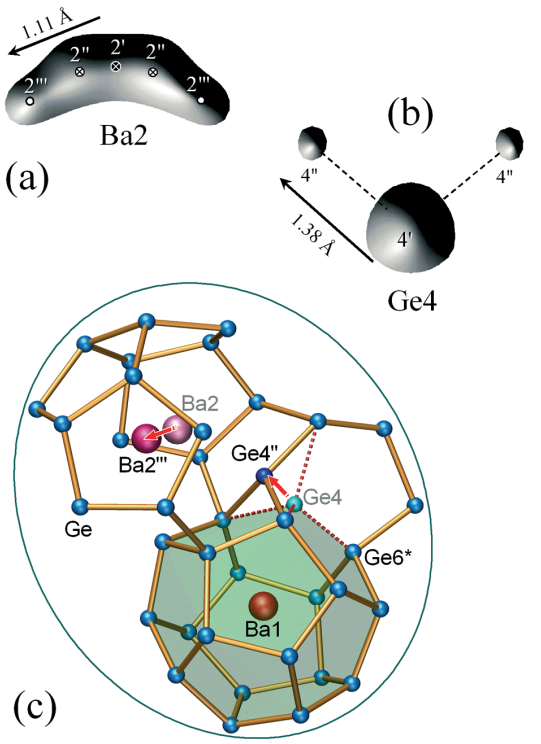

Fig. 2: Difference electron density isosurfaces of Ba2 (a) and Ge4 (b) at 165 K. The split atoms sites of Ba2 and Ge4 are labeled 2′, 2″, 2‴ and 4′, 4″, respectively. The model (c) illustrates the Ge4–Ge6 bond breaking associated with the displacement of the Ba2. Also bond breaking at three bonded (3b)Ge$^-$ species at Ge4" and Ge6 appear.*

Only the germanium at the Ge4 site (Wyckoff position 12*d*) is influenced significantly by the transformation. Below ~250 K, close to the main site (called Ge4′ at low temperatures), two Ge4″ satellite sites at 24*e* appear. The beginning of the occupation of Ge4″ sites at about 250 K define the first step *S0* of the transformation. The shifting of these two positions has to be correlated, because Ge4 is a next neighbor to Ba2. Between *S0* (250 K) and *S1* (225 K) the occupation of Ge4″ site varies from 0 % to 1.7 %. An equivalent change of the elongated distribution at Ba2 has not been observed. Therefore, we assume that the first Ge4″ shifted atoms are neighbors of the Ba2″ split sites. Below T_{S1}(down) the occupation of Ge4″ is correlated to the appearance and occupation of a second split atom site, i.e. Ba2‴ (Fig. 1). The occupancy of the Ge4″ site increases from 1.7 % at 225 K to 14.6 % at 95 K, while the occupancy of the Ba2‴ site increases from 0 % to 13.3 %. Both effects are reversible and show hysteresis. During cooling at about 180 K ($\approx T_{S2}$(down) the increasing number of Ba2 atoms at the Ba2‴ split atom site provokes the displacement of the neighbored Ba3 atoms, which further influences the displacement of the Ba1 atoms.

In order to describe the correlated displacement of Ge4 and Ba2 (one of two possibilities) through the transition, we have used a short-range model described in the lower symmetry space group *R*3. The model is presented in the next section. The significant displacement of Ge4 causes the bond breaking at Ge4–Ge6. Therefore, three-bonded (3b)Ge$^-$ electron acceptors with sp^3 configuration are formed at Ge4″ and Ge6 sites, for details see the structural fragment in Fig. 2.

The negative species (3b)Ge$^-$ with dangling bonds occupy a larger volume than the neutral species (4b)Ge^0. Therefore, the appearance of (3b)Ge$^-$ below 250 K can explain the anomalous behavior of the unit cell parameter, which increases as a function of decreasing temperature, going through the phase transition (see Fig. 3a). According to the Zintl-Klemm concept, the forma-

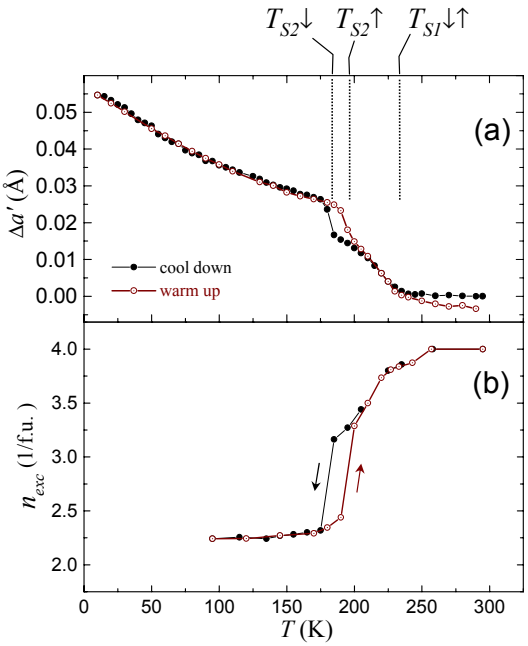

Fig. 3: (a) Change of the unit-cell parameter (Δa') of Ba_6Ge_{25} as function of temperature (T) obtained from powder X-ray diffraction data. Δa'(T) is the difference to the unit cell parameter of a hypothetical phase with no phase transition, assuming a linear dependence on temperature. $\Delta a'(T) = a(T) - a'(T)$; $a' = a_o + \gamma T$, a_o = 14.4764 Å, $\gamma = 2.711\times10^{-4}$ ÅK^{-1}. T_{S1} and T_{S2} indicate the two steps in the phase transition on cooling (↓) or heating (↑). (b) Temperature dependence of the number of excess electrons n_{exc} per formula unit using the Zintl-Klemm counting rule in combination with the occupancy of the Ge4" site.

tion of new species (3b)Ge^- leads to the reduction of excess charges from 4 e^- (at $T > 250$ K) to about 2.24 e^- per formula unit at 95 K. This is illustrated in Fig. 3b, where the concentration of excess electrons, n_{exc}, is plotted as a function of temperature. The variations of $n_{exc}(T)$ and the lattice irregularities induced by the transformation influence all physical properties. The Ge–Ge bond breaking combined with the reduction of excess-charges represents a solid-state chemical reaction. To our knowledge, this is the first observation where covalent Ge–Ge bonds are broken at low temperatures.

Influence of cage distortions on the band structure and optical properties in Ba_6Ge_{25}

In order to perform band-structure calculations, ordered structural models have been constructed. In the previous section it was shown that above the phase transition of Ba_6Ge_{25} the atoms are placed at their average, high symmetry positions, within the space group $P4_132$ (no. 213). This is in good agreement with the structural data, where the electron-density distributions are nearly symmetrical for most of the atoms. An exception is Ba2, but here the displacement is relatively small in comparison with the displacement below the structural phase transition. Below the phase transition the atoms shift to split atom sites, as described in the previous section. The most remarkable structural feature is the shift of a fraction of Ge4 atoms to the distant split atom sites. The ordered structural model is constructed within the space group $R3$ (no. 146). The high and low temperature models are referred to as the HT and the LT model, respectively. In the LT model three out of twelve Ge4 atoms per unit cell are shift-

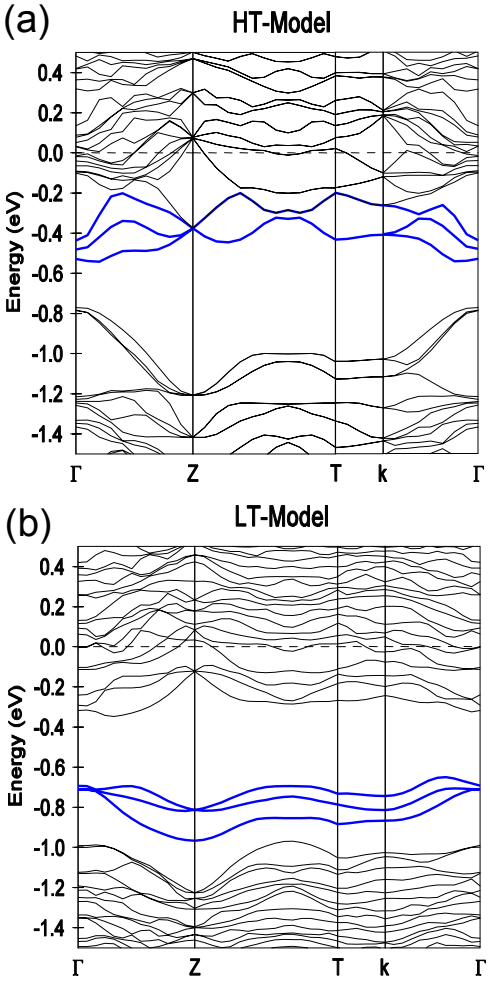

Fig. 4: Electronic band structures for the HT (a) and LT (b) models. The three bands at the bottom of the conduction-band region in the HT model, emphasized by the bold blue lines, are shifted onto the top of the valence-band region in the LT model.

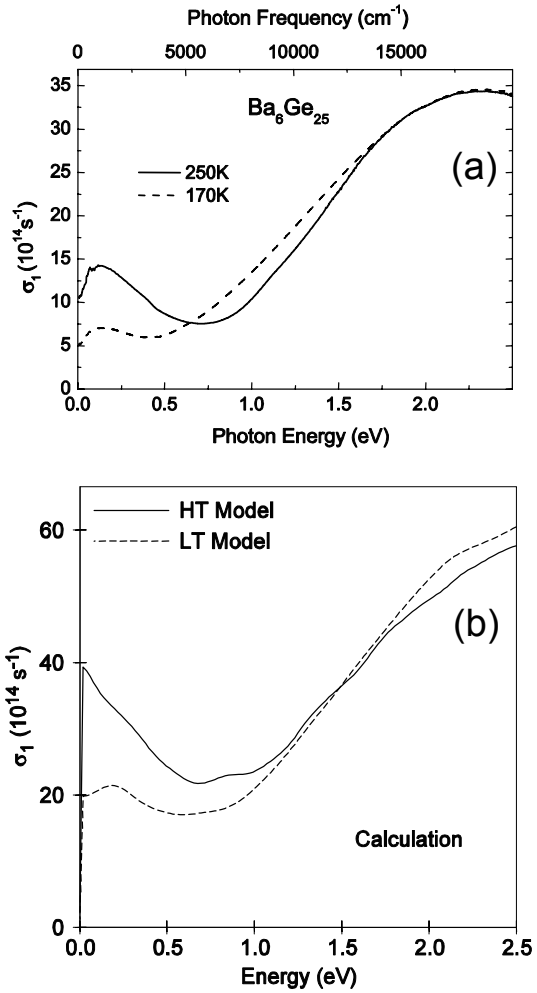

Fig. 5: (a) Measured optical conductivity of Ba_6Ge_{25} at a temperature above (T = 250 K) and below (T = 170 K) the phase-transition temperature. A shift of spectral weight towards higher energies occurs below the phase-transition temperature. (b) Theoretical calculation of the absorptive part of the optical conductivity. Calculations are based on band-structure calculations for the HT and the LT model (Fig. 9).

ed to one of the Ge4″ sites, located inside large bipyramids formed by Ba atoms. These sites are very close to Ba2 average sites. To avoid non-physical short distances, the corresponding Ba2 atoms are simultaneously shifted to the Ba2‴ sites (Fig. 2). In this way, the fraction of atoms at Ge4″ and Ba2‴ sites agree with the occupations of the corresponding split atom sites obtained from the structure refinement. All the other atoms in the LT model are distributed among the sites within *R*3 space group, so that the distribution approximately agrees with the experimentally observed split atom site occupations in the space group $P4_132$.

The electronic band-structure calculations have been performed within the local density approximation (LDA) using the LMTO method within the atomic sphere approximation. The optical conductivity has been calculated using standard formulas. The most distinctive effect on the electronic band structure (Fig. 4) is the shifting of three bands from the bottom of the conduction region in the HT model to the top of the valence region in the LT model. This is a consequence of the Ge–Ge bond breaking, since Ge4 is displaced towards one of the Ge4″ sites. This band-structure rearrangement strongly influences the optical conductivity. The number of initial states for the optical transitions with energies ≤ 0.5 eV is reduced, as a result of the shifting of the three bands. As a consequence, the optical spectral weights are shifted above the phase transition temperature towards higher energies (Fig. 5), which is in agreement with the experimental observation [10, 11].

The displacement of Ba2 alone cannot explain the shift of the optical spectral weights [12]. Only the newly discovered breaking of Ge–Ge bonds can account for the modifications of the optical properties induced by the phase transition. Besides the optical properties the superconductivity and the interplay with the structural phase transition have been analyzed [13].

Electron Spin Resonance of Eu^{2+} in Eu doped Ba_6Ge_{25}

We performed electron spin resonance (ESR) investigations of the Eu^{2+} spin in $Ba_{6-x}Eu_xGe_{25}$ with $x = 0.03$, 0.05, 0.1, 0.2 and 0.4 [14] where the Eu^{2+} ions randomly occupy the Ba1 and Ba3 sites. The ESR line width ΔB of these ions reflects the magnetic relaxation, which in turn measures the interaction between the Eu-4*f* states and the conduction electrons. Two kinks in the temperature dependence of ΔB have been found: one near the structural phase transition at $T \cong 175$ K and another at $T \cong 60$ K, see Fig. 6.

The temperature dependence of the structural details, especially those of the Ge_{20} pentagon dodecahedral cage and the Ba displacements [7], proves to be consistent with the ESR results. The shifting of the structural phase transitions by Eu-doping towards lower temperatures, as seen in the electrical resistivity, does not produce correspon-

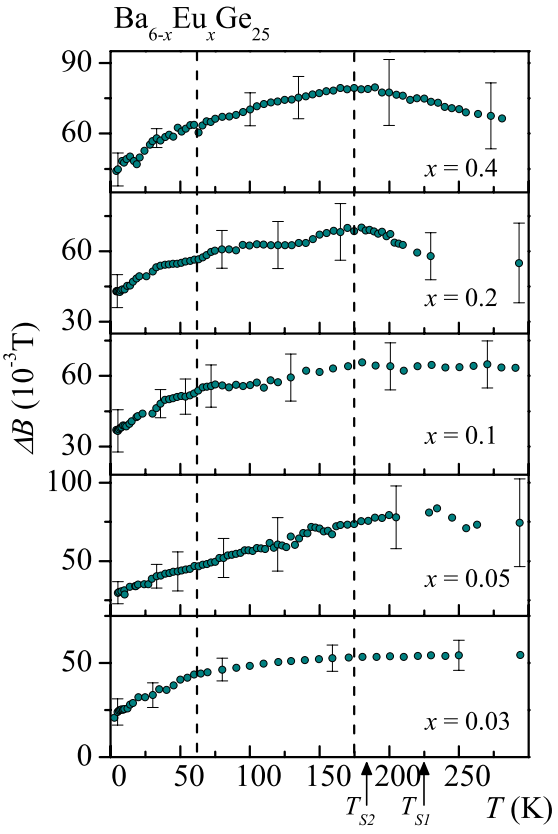

Fig. 6: Temperature dependences of the ESR line width ΔB. The vertical dashed lines mark those temperatures where the average slope of ΔB changes. The arrows at T_{S1} and T_{S2} mark the temperatures between which a two-step reconstructive structure transformation occurs.

ding changes of any ESR parameters. Treating the observed spectra as ESR of local moments in a metallic host, the slope changes in $\Delta B(T)$ are due to changes of the local-moment, conduction-electron exchange as well as to changes of the electronic density of states at the Fermi energy. The latter has been shown to be the result of changes in electronic band structure [11]. This is detected by ESR most effectively by the Eu^{2+} ion at the Ba1 site.

$Ba_{8-x}Eu_xGe_{43}\square_3$ ($x \leq 0.6$)

The defect clathrate $Ba_8Ge_{43}\square_3$, where $\square$ symbolizes a vacancy, crystallizes in a structure close to the clathrate type-I, with three Ge atoms missing in the covalent germanium framework [15, 16]. The ordering of the defects leads to the formation of a superstructure, which is accompanied by a doubling of the unit-cell constant [17]. In crystals with partial substitution of Ba by Eu no superstructure was detected [18]. $Ba_{8-x}Eu_xGe_{43}\square_3$ ($x \leq 0.6$) exhibits a defect clathrate type-I structure with Eu randomly replacing some of the Ba atoms in the smaller cages. Polycrystalline $Ba_8Ge_{43}\square_3$ samples are synthesized from the elements by high-frequency induction melting in open glassy carbon crucibles and subsequent annealing [17]. For the synthesis of polycrystalline samples with $x = 0.3, 0.6$ a high-pressure and -temperature technique has been applied.

Investigations of electrical-transport properties of all three compositions ($x = 0, 0.3, 0.6$) revealed a metal-like temperature dependence of the resistivity, $\rho(T)$ (Fig. 7). Below approximately 10 K, ρ becomes temperature independent. The residual resistivity ratios $RRR = \rho_{300K}/\rho_{2K}$ are relatively small for all samples and decrease with increasing Eu content. This finding suggests that disorder scattering due to Eu substitution and Ge defects plays a significant role in the material.

In order to identify the magnetic ground state of the Eu-containing samples, measurements of magnetic susceptibility have been performed. At temperatures $T > 50$ K, the data can be well described by a modified Curie-Weiss law, $\chi = \chi_0 + C/(T-\Theta)$. In the case of the sample with $x = 0.3$ least-squares fits yield a temperature-independent susceptibility $\chi_0 = -2.11(3)\times10^{-6}$ emu mol^{-1}, a Weiss temperature $\Theta = -1.1(1)$ K and an effective magnetic moment of $\mu_{eff} = 7.71\ \mu_B$ for Eu as derived from C (values for a field of 70 kOe). For $x = 0.6$, the corresponding values are $-2.86(2)\times10^{-6}$ emu mol^{-1}, with Q set to zero, and $\mu_{eff} = 7.93\ \mu_B$. The two values of the paramagnetic moment are close to that of the $^8S_{7/2}$ ground state of Eu with $4f^7$ configuration (7.94 μ_B), i.e., europium is present as Eu^{2+}. Remarkably, χ_0 is

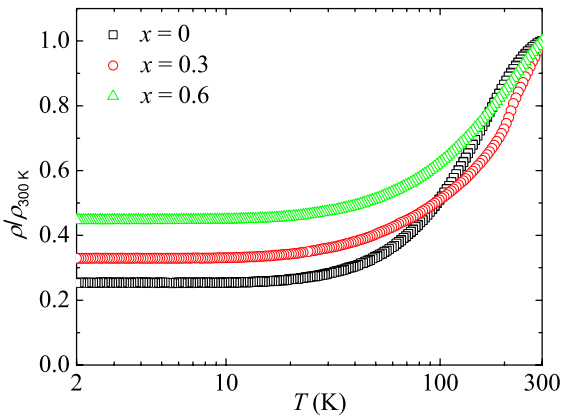

Fig. 7: Temperature dependence of electrical resistivity ρ(T) of the clathrate $Ba_{8-x}Eu_xGe_{43}\square_3$ (x = 0, 0.3, 0.6).

approximately 4 times larger than the sum of the diamagnetic increments. This effect could be due to Larmor contributions to the diamagnetism of this clathrate or to crystalline electric field effects. The small values of Θ imply weak interactions between the magnetic moments. Consequently, no long-range magnetic ordering is observed down to 1.8 K.

In Fig. 8 a plot of the temperature dependence of the specific heat $C_p(T)$ of $Ba_{8-x}Eu_xGe_{43}\square_3$ (x = 0, 0.3, 0.6) is shown. The dashed line marks the associated Dulong-Petit value, $DP = 3Rn$, where R is the gas constant and n the number of atoms per unit cell. While C_p for both the $x = 0$ and $x = 0.6$ sample reaches this value near room temperature, the x = 0.3 sample has a significantly reduced C_p. The observed deviation corresponds to a mass deficiency of ≈ 6.4 % and is attributed to the uncertainty in the determination of the mass of this sample (total mass only < 1 mg). At temperatures above 10 K, the C_p (T) curves are in satisfactory agreement, a finding which only holds when the mass of the x = 0.3 sample is corrected with respect to the validity of the Dulong-Petit law. This indicates the same phonon contributions to $C_p(T)$. However, at lower temperatures the heat capacity $C_p(T)$ of the Eu-containing samples deviates considerably from the pure barium clathrate (inset of Fig. 8). For the doped samples a broad hump is observed below 10 K, and the intensity of this effect rises with increasing Eu content. Applying a magnetic field shifts the hump to higher temperatures [19]. We attribute this anomaly to a Schottky contribution that originates from

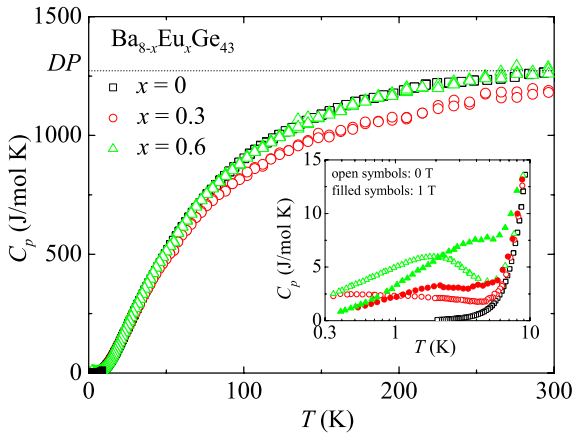

Fig. 8: Specific heat C_P vs. temperature T for $Ba_{8-x}Eu_xGe_{43}\square_3$ (x = 0.0, 0.3, 0.6). The dashed line marks the Dulong-Petit value $DP = 3nR$. The inset shows the low temperature part both in zero magnetic field and 1 T.

the energy-level splitting of the ground state octet of the Eu^{2+} due to the crystal-electric and magnetic fields. Although the ground state of Eu^{2+} is generally assumed to be $(4f^7)$ $^8S_{7/2}$ and thus rotational invariant, admixtures of higher lying states allow for a splitting of the degenerate ground state energy levels in a crystal-electric field. The overall splitting being some hundred mK to several K and may be enlarged by internal and external magnetic fields.

For an analysis of the data we assume C_p to be a sum of three contributions: $C_p = C_{ph} + C_{el} + C_s$ with C_{ph} being the phononic, C_{el} the electronic and C_s the field-dependent Schottky specific heat. An estimate of C_{el} in a free-electron model shows that it is small in the temperature range of interest and may therefore be neglected. Due to the unknown initial ground-state splitting it is impossible to calculate C_s. In order to separate C_s and C_{ph} we need to determine C_{ph} at low T. For this sake we fitted a sum of one Debye and two Einstein terms to the zero field $C_{ph}(T)$ data between 10 K and 300 K. The Debye term approximates the acoustic phonon modes, the first Einstein term the optic modes of the Ge framework. The second Einstein term was added in order to account for thermal vibrations of the Eu and Ba cations inside the cages. The resulting Debye temperatures Θ_D are 167 K and 156 K for the x = 0.3 and the x = 0.6 sample, respectively. As Einstein temperatures $\Theta_{E1,2}$ we found Θ_{E1} = 343 K, Θ_{E2} = 60 K (x = 0.3) and Θ_{E1} = 303 K, Θ_{E2} = 61 K (x = 0.6). These values do not differ significantly indicating a negligible influence of the Eu content on the spectrum of the lattice vibrations.

Subtracting the estimated $C_{ph}(T)$ from $C_p(T)$ we obtain the magnetic field dependent $C_s(T)$. The results for x = 0.6 are plotted in Fig. 9.

The corresponding entropies per mole Eu are $(1.1\pm0.1)R\cdot\ln 8$ and $(1.4\pm0.1)R\cdot\ln 8$ for the x = 0.3 and the x = 0.6 samples, respectively. The deviations from the expected value $R\cdot\ln 8$ may be due to uncertainties in measuring $C_p(T)$, inaccuracy of x, the neglecting of $C_{el}(T)$ and errors in the estimate of $C_{ph}(T)$. $C_s(T)$ resembles a Schottky function. With increasing field the temperature of the maximum T_{max} shifts towards higher T, which corresponds to an increase of the overall splitting of the $^8S_{7/2}$ manifold. Determining the level scheme by fitting the Schottky anomaly was not possible, as the disordered Eu distribution leads to a position-dependent internal magnetic field. Approximating the problem by a sum of several Schottky functions

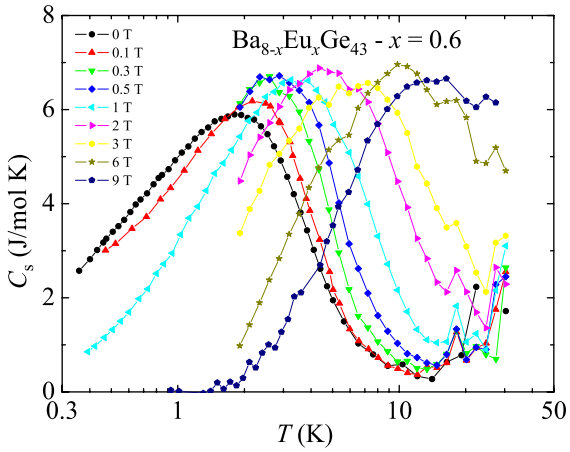

Fig. 9: Schottky contribution to the specific heat for $Ba_{8-x}Eu_xGe_{43}\square_3$ (x = 0.6) in various magnetic fields.

fails due to a too large number of unknown parameters. However, for a qualitative test the field shift of T_{max} may be compared to that expected for a simple $\pm s$ spin doublet. For the x = 0.6 sample, a plot of T_{max} vs. $\mu_0 H$ reveals an approximately linear dependency (not shown) as expected for a doublet with initial splitting ΔT = 5.0 K and spin ± 5/2. The results for the x = 0.3 sample are ΔT = 4.0 K and s = ± 3.7/2. These values are reasonable for Eu^{2+} and support our interpretation of the low-temperature contribution to C_p to be caused by a splitting of the $^8S_{7/2}$ ground state octet.

Charge-carrier properties of α- and β-$Eu_8Ga_{16}Ge_{30}$

The original idea to substitute Yb or Sm for Ba to create *f*-electron intermediate valence was not successful, and it appears that Eu is the only rare-earth element that can be substituted for Ba. α- and β-$Eu_8Ga_{16-x}Ge_{30+x}$ are still the only examples in the literature where the cation sites are fully occupied by a rare-earth element. These two clathrate compounds have been investigated at the MPI CPfS, and we refer to our previous scientific reports for detailed structural and physical properties [1, 2]. In the following we report on thermal conductivity and tunneling states of α- and β-$Eu_8Ga_{16-x}Ge_{30+x}$, both topics being of considerable interest for the thermoelectric community.

Thermopower data and band-structure calculations of α- and β-$Eu_8Ga_{16}Ge_{30}$ suggest that the effective mass (m^*) of the charge carriers in the β phase is 3 to 4 times larger than in the α phase. We have investigated this difference in more detail and the low-temperature specific heat (C_p) has been measured for one α sample and one β sample [20], referred to as α6 and β3 in the following. The result is plotted in Fig. 10 as C_p/T vs T^2. The straight solid lines correspond to fits of the relation $C_p/T = \gamma + \beta T^2$ to the data where the Sommerfeld coefficient γ represents the electronic contribution and the $\beta \cdot T^2$ term the phononic contribution with $\beta = 12\pi^4 \cdot N \cdot R/(5\theta)$. θ_D is the Debye temperature, N and R are the concentration of atoms and the gas constant, respectively. In order to suppress contributions from the magnetic ordering, $C_p(T)$ was measured in a magnetic field B = 9 T. The magnitude of γ confirms that m^* in the β phase is larger than in the α phase. Dependent on whether a normal or spin-polarized free-electron model is used, the density-of-states effective masses are calculated from the charge-carrier density (n) and γ to be 0.75 m_0 (1.2 m_0) and 4.6 m_0 (6.3 m_0) for the α6 and β3 sample, respectively. The numbers in parentheses are for the spin polarized free-electron model.

The inset of Fig. 10 shows the change of C_p/T as a function of magnetic field at 0.4 K. Even at the highest magnetic field of 9 T C_p/T continues to decrease slightly with increasing field. Therefore, it cannot be excluded that the magnetic ordering contributes to C_p/T and that the values of and the density of states are slightly overestimated. θ_D calculated from β is 251 K and 159 K for α6 and β3, respectively.

Likewise m^* has an influence on both the lattice thermal conductivity (next section) and the mag-

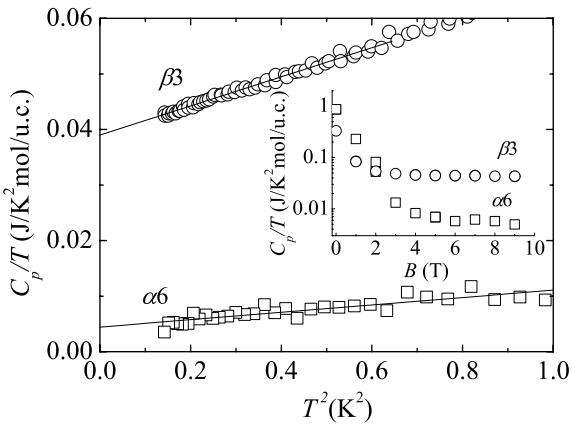

Fig. 10: Specific heat (C_p) divided by temperature (T), as function of T² for α6 (squares) and β3 (circles), measured in a magnetic field of 9 T. The inset shows C_p(T)/T as function of the magnetic field (B) at 0.4 K.

netic properties. It is believed that the ferromagnetic ordering, at approximately 10 K and 35 K for the α and β phase, respectively [21], is due to the indirect Rudermann-Kittel-Kasuya-Yosida (RKKY) interaction. In a free-electron model the RKKY interaction takes the form $J_{RKKY} \propto m^* \cdot \Sigma_j (2k_F \cdot R_{ij} \cdot \cos(2k_F \cdot R_{ij}) - \sin(2k_F \cdot R_{ij}))/R_{ij}^4$, where R_{ij} is the distance between ion i and j and k_F is the Fermi wavevector. For both structures, $\Sigma_j (2k_F \cdot R_{ij} \cos(2k_F \cdot R_{ij}) - \sin(2k_F \cdot R_{ij}))/R_{ij}^4$, is nearly of the same magnitude because of similar average Eu–Eu distances and similar k_F values. Since the magnetic ordering temperature $T_c \propto J_{RKKY}$, the difference between the α and β phase ($T_c(\beta) \approx 3.5\ T_c(\alpha)$) can, therefore, almost entirely be ascribed to the larger m^*-value in the β phase compared to that in the α phase.

Thermal conductivity of α- and β-$Eu_8Ga_{16}Ge_{30}$

The lattice thermal conductivity (κ_L) of clathrates has been intriguing since the discovery of a 'glasslike' magnitude and temperature dependence of $\kappa_L(T)$ in β-$Eu_8Ga_{16}Ge_{30}$ and $Sr_8Ga_{16}Ge_{30}$ [22, 23] as opposed to normal 'crystal-like' $\kappa_L(T)$ in other clathrates. The glasslike $\kappa_L(T)$ of β-$Eu_8Ga_{16}Ge_{30}$ and $Sr_8Ga_{16}Ge_{30}$ has previously been explained by a combination of resonant scattering of cation vibrations and scattering of phonons from cation tunneling states [23, 24]. However, it would be expected that simple disorder with four split positions would result in a highly localized density of tunneling states leading to a $\kappa_L(T)$ similar to what is observed for resonant scattering. Instead, we suggest that phonon-charge-carrier scattering should be considered when describing $\kappa_L(T)$ at the lowest temperatures [25]. This model can account for differences in the low-temperature $\kappa_L(T)$, not only among α- and β-$Eu_8Ga_{16-x}Ge_{30+x}$ samples, respectively, but also for the large difference in $\kappa_L(T)$ between the α- and β-phase. The difference in $\kappa_L(T)$ at intermediate and high temperatures both among α- and β-$Eu_8Ga_{16-x}Ge_{30+x}$ samples and between the α- and β-phase is attributed to differences in the coupling between resonant scatterers and the heat-carrying acoustic phonons. This does not exclude the existence of tunneling states (see next section), but their influence on $\kappa_L(T)$ in β-$Eu_8Ga_{16}Ge_{30}$ appears to be insignificant [26].

Fig. 11 shows $\kappa_L(T)$ for one α sample and one β sample, in the following referred to as $\alpha 7$ and $\beta 1$, respectively. The solid lines imposed on the data points are model calculations using

$$\kappa_L = \frac{v_p}{3} \int_0^{\frac{\theta_D}{T}} C(T,z) \cdot l(T,z) dz ,$$

where v_p is phonon velocity, θ_D is the Debye temperature, C is the fractional specific heat of phonons with $z = \hbar v_p q/(k_B T)$, and q is the phonon wavenumber. l is the total mean free path from different scattering mechanisms. In our model we use

$$l = (l_{p\text{-}c}^{-1} + l_{res}^{-1} + l_{ray}^{-1} + l_{Cas}^{-1})^{-1} + l_{p,min} ,$$

where $l_{p\text{-}c}$ refers to phonon charge-carrier scattering, l_{Cas} to Casimir/boundary scattering (low temperature), l_{res} to resonant scattering of phonons on the cations (intermediate temperatures), l_{ray} to Rayleigh/Mass difference/defect scattering (up to room temperature) and $l_{p,min}$ to a parameter preventing l from becoming unphysically low. Theoretically, phonon charge-carrier scattering can have a strong dependence on the mean free path of the charge carriers (l_c).

To emphasize that $\kappa_L(T)$ at low temperatures can be explained by phonon-charge-carrier scattering, κ_L(3 K) has been calculated as a function of l_c for the α phase, and the result is plotted as the solid curve in the inset of Fig. 11. Here, the only adjustable parameter is l_c. The other parameters were

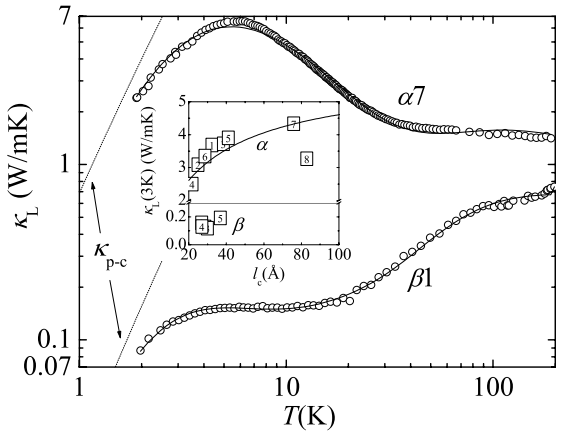

Fig. 11: Lattice thermal conductivity (κ_L) as function of temperature (T) for the two samples $\alpha 7$ and $\beta 1$. Solid curves are fits of a model described in the text to the observed data. Dotted lines ($\kappa_{p\text{-}c}$) represent the lattice thermal conductivities of this model, if only phonon charge-carrier scattering is present. Inset shows κ_L(3 K) as function of the mean free path of the charge carriers (l_c) of the α- and β-$Eu_8Ga_{16-x}Ge_{30+x}$ samples. The numbers in the data points refers to the sample numbers.

kept constant at the values that were fitted for $\alpha 7$. It is seen that, with the exception of κ_L(3 K) for $\alpha 8$, the model tracks the data, and it can be concluded that the variation of κ_L at 3 K among different α samples is dominated by the variation of l_c. For the β samples the variation of κ_L is much smaller, because l_c only varies slightly among different β samples.

Tunneling states in β-$Eu_8Ga_{16}Ge_{30}$

Large static atomic displacement parameters for guest atoms suggest the possibility of tunneling states in type I clathrates [21, 23]. Here, we present strong evidence for the existence of tunneling states in β-$Eu_8Ga_{16}Ge_{30}$ [27], provided by elastic constant measurements via resonant ultrasound spectroscopy (RUS) [28].

At low temperatures an unusual softening of the material has been observed, which could not be explained by taking into account the elastic response of the low-frequency Einstein modes, corresponding to the vibrations of Eu atoms. The simple two-level tunneling model could explain the elastic response, but is inconsistent with the specific-heat measurements, where no anomaly corresponding to the tunneling energy is observed [29]. However, a four-well tunneling model which is in accordance with both the four split sites for Eu2 atoms, deduced from the neutron-scattering and X-ray-scattering data [21, 29, 30] as well as specific heat can explain the elastic response of β-$Eu_8Ga_{16}Ge_{30}$.

The nuclear density distribution obtained from neutron scattering reveals that the Eu atoms are almost completely expelled from the cage centers and evenly distributed among four symmetrically related split atom sites in the plane. In accordance with these experimental data the four-well potential can be modeled as

$$V(\rho,\phi)=\frac{V_0}{\rho^2}(1+\cos(4\phi))+\frac{V_1}{\rho^2}+\frac{1}{2}K\rho^2.$$

The harmonic oscillator (HO) potential of the last term is modified by the four-well potential term: V_0 is the potential barrier in the azimuthal direction; V_1 term determines the distance from the cage center to the four minima in the potential. There is no tunneling of Eu through the cage center.

The sum V_0+V_1 is determined under the condition that the radial wave-function maximum is in agreement with the Eu2 displacement from the cage center as deduced from neutron-scattering experiments. V_0 is then adjusted to fit the specific-heat data. The resulting azimuthal potential and the energy scheme is presented on Fig. 12. The lowest states form two four-level systems (FLS) with the tunneling energies Δ_1 = 0.05 K and Δ_2 = 0.85 K, separated by the gap Δ_3 = 22 K. The elastic properties of β-$Eu_8Ga_{16}Ge_{30}$ may be understood if decoherence effects for the lowest FLS_1 are taken into account. It may be shown that in the temperature range of interest, the coherence of FLS_1 is destroyed, because the tunneling in FLS_1 is very slow. Then the observed low-temperature minimum in the elastic constants obtained from the RUS measurements is explained by the elastic response of FLS_2. Using the linear response theory, it is described [4] by

$$\Delta c_\mu(T)=-\frac{n_c}{Z(T)}\exp\left(-\frac{\Delta_3}{k_BT}\right)\left[\frac{2\gamma_{\mu 2}^2}{\Delta_2}\sinh\left(\frac{\Delta_2}{k_BT}\right)+\frac{2\gamma_{\mu 2}^2}{k_BT}\right],$$

where $\gamma_{\mu 2}$ is the interaction strength of the quadrupolar coupling of FLS_2 with the elastic strains, n_c is the FLS concentration, and $Z(T)$ is the partition function. Fitting the elastic constant data leads to $\gamma_{\mu 2} \approx 0.073$ eV. The elastic constant curves are shown in Fig. 13. The calculated values agree well with the experimental data.

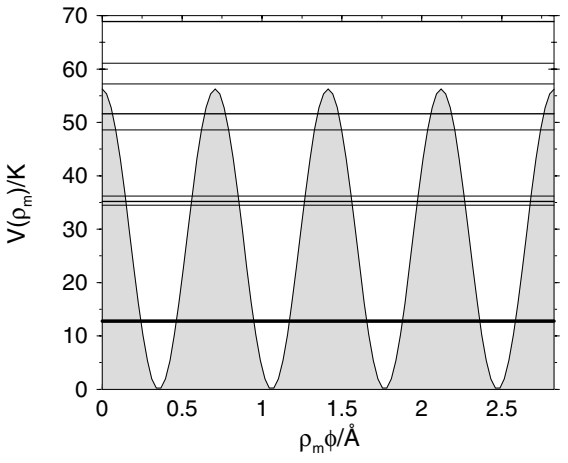

Fig. 12: The four-well potential along the circle of ρ_{max}, the radial distance of maximum nuclear density for Eu clathrate. Energy eigenvalues are plotted as horizontal lines. The ground state consists of FLS_1, shown as the thickest line. Medium thick lines correspond to the doubly-degenerate and thin lines to the non-degenerate states. The energy units are given in Kelvin.

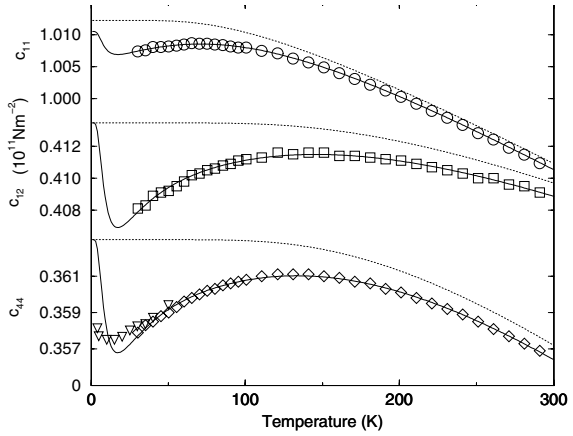

Fig. 13: The fit of the elastic constants of Eu clathrate. The background variation, shown by the dashed lines, corresponds to Varshni function [37]. The experimental data are from ref. [27].

Electronic band structure and optical properties of α-$Eu_8Ga_{16-x}Ge_{30+x}$

We have measured the near normal incidence reflection on α-$Eu_8Ga_{16-x}Ge_{30+x}$ of the particular composition with $x = 0.42$ in a wide spectral region (7 meV – 30 eV) at temperatures above and below the ferromagnetic phase transition temperature, T_C = 10.5 K [14]. The low-energy Drude type of the optical conductivity, cf. Fig. 14, is characterized by a very low charge-carrier density, $n_{opt} \cong 0.22\ e^-$/(unit cell), in accordance with the results of Hall-effect

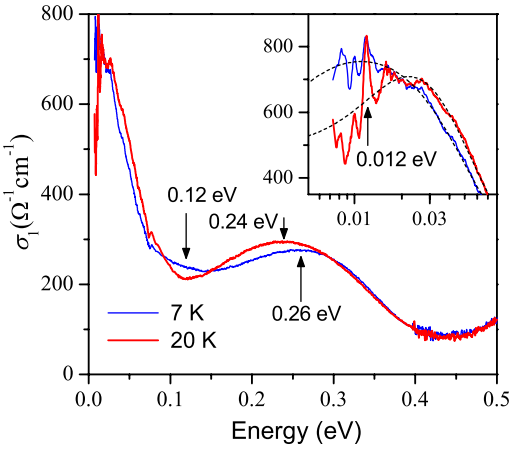

Fig. 14: Optical conductivity spectra of α-$Eu_8Ga_{16-x}Ge_{30+x}$ ($x = 0.42$) at $T = 7$ K and 20 K, below, and above T_C, respectively. Arrows and inset emphasize pronounced changes to $\sigma_1(\omega, T)$ when changing T across T_C. Inset: Enlarged view of the low-energy part with a phononic feature at 0.012 eV. Thin dashed lines describe the spectra with a Drude-Lorentz oscillator.

measurements [21]. The low-energy region 0.1 – 0.4 eV is characterized by transitions within the lower end of the conduction band, in agreement with band-structure calculations which also correctly predict the valence-conduction band gap as observed (> 0.4 eV) [31]. At energies between 10 and 100 meV, pronounced broad peak structures are observed and assigned to excitations from disorder-derived bound states within the band gap, reflecting the random distribution of the Ga- and Ge-atoms in the clathrate network [25]. By lowering the temperature across T_C, the shifting of the Fermi level in the exchange-split conduction band causes the peak structures in the optical conductivity to change in shape and position at energies below 0.4 eV, whereas the spectral weight is conserved in this energy region.

New clathrates with ordered substitution in cationic sites

Many attempts to synthesize rare-earth containing clathrates were unsuccessful. Only two modifications, α-$Eu_8Ga_{16-x}Ga_{30+x}$ with clathrate type-VIII structure stable in a narrow temperature range close to 650 ºC and β-$Eu_8Ga_{16-x}Ga_{30+x}$ obtained from the melt, are characterized by a full occupation of the cationic sites by a rare-earth element. Another possibility to obtain rare-earth containing clathrates is partial substitution of cationic sites. Recently, some clathrate type-I compounds with guest sites, that are partially occupied by a rare-earth element, have been reported: $Sr_4Eu_4Ga_{16}Ge_{30}$ [23], $Ba_6Eu_2Cu_4Si_{42}$, $Ba_6Eu_2Al_8Si_{36}$, $Ba_6Eu_2Cu_4Si_{38}Ga_4$ [32], $Ba_6Ce_2Cu_4Si_{42}$ [33] and $Ba_6Ce_2Au_4Si_{42}$ [34]. In case of $Ba_6Ce_2Au_4Si_{42}$ later work has shown that the clathrate material did not contain cerium in a detectable quantity [35]. In this section the results of the partial substitution of the cationic sites in potassium containing clathrates and in the orthorhombic clathrate $Ba_8Cu_{16}P_{30}$ is discussed.

Bulk materials of europium-containing clathrates $K_6Eu_2Ga_{10}Ge_{36}$, $K_6Eu_2Zn_5Ge_{41}$ and $K_6Eu_2Cd_5Ge_{41}$ were prepared by a two-step ampoule synthesis. Stoichiometric quantities of the starting materials were enclosed into tantalum containers under purified argon atmosphere. The containers were heated in a high-frequency furnace. The result is a mixture of binary compounds and germanium, which was grinded, pressed into a pellet and annealed under

the same conditions. This procedure was repeated several times. All samples were characterized by X-ray powder diffraction. The chemical composition obtained from single-crystal structure refinement was checked by energy-dispersive X-ray absorption analysis (EDX). Measurements were performed on the single crystals and small crystallites of bulk samples.

The measurements of the Eu-L_{III} X-ray absorption spectrum (XAS) of powdered samples were performed in transmission geometry at the EXAFS II beamline E4 of the HASYLAB at DESY. The synchrotron beam is monochromatized by a Si (111) double-crystal monochromator which yields an experimental resolution of approximately 2 eV at the Eu-L_{III} edge of 6977 eV. The experimental data were recorded simultaneously for Eu_2O_3 as an external reference compound. All of the investigated Eu-substituted compounds crystallize with clathrate type I (*Pm*$\bar{3}$*n, cP54*) structure: $K_6Eu_2Ga_{10}Ge_{36}$ (a = 10.7441(6) Å), $K_6Eu_2Zn_5Ge_{41}$ (a = 10.7442(8) Å), $K_6Eu_2Cd_5Ge_{41}$ (a = 10.8349(6) Å). No homogeneity ranges were observed for any compound. The dodecahedral cationic sites are occupied by europium ions and the tetracaidecahedral by the potassium ions. All positions of the anionic network are characterized by a mixed occupation of gallium/zinc/cadmium and germanium atoms. All of the compounds are Curie-Weiss paramagnets with ferromagnetic ordering at temperature below 10 K. The magnetic moment of Eu is close to 7.9 μ_B. This value corresponds to the spin only state of the $4f^7$ electronic configuration and is also confirmed by XAS spectroscopy. The temperature dependence of the electrical resistivities indicates that all the clathrates are semiconductors.

Orthorhombic $Ba_8Cu_{16}P_{30}$ is closely related to the clathrates with a group 14 element occupying the anionic network [36]. The structural relation between orthorhombic $Ba_8Cu_{16}P_{30}$ and the clathrate type-I structure (see Fig. 15) can be described by the following transformations: $a_o = a_c$ = 14.117 Å, $b_o = a_c$ = 10.093 Å, $c_o = 2a_c$ = 28.022 Å. In contrast to clathrates with type-I structure the anionic framework of $Ba_8Cu_{16}P_{30}$ is completely ordered, i.e. each copper is tetrahedrally coordinated by phosphorus and this is probably also the origin of the superstructure formation. Samples with nominal compositions $Ba_{8-x}Eu_xCu_{16}P_{30}$ (x = 0 – 2 with 0.5 steps) were synthesized by a method similar to the one used for the potassium clathrates described above.

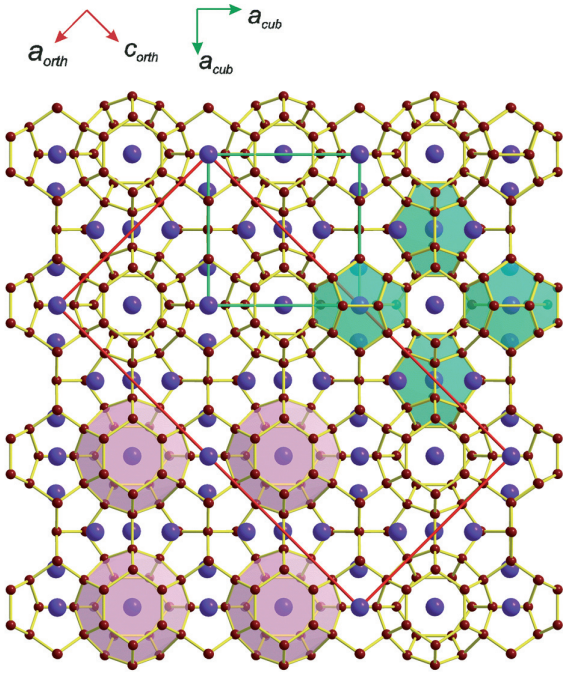

Fig. 15: Relation between the conventional unit cell of the type-I clathrate structure and the unit cell of the superstructure of $Ba_8Cu_{16}P_{30}$, marked by the green and red lattice, respectively. Green dodecahedral cationic sites are occupied almost entirely by europium ions and purple tetracaidecahedral nearly entirely by potassium or barium ions.

The resulting mixture contains numerous silvery plate-like crystals, which are stable in air for a long period of time, and resists the treatment with diluted hydrochloric acid (1:1). Powdered samples are grey, and visible reaction with air is observed within a few days. Single-crystal X-ray investigations of the samples show a preferential occupation of europium at the centre of the relatively smaller dodecahedral cavities. The magnitude and temperature dependence of the magnetic susceptibility of $Ba_8Cu_{16}P_{30}$ is consistent with a superposition of a diamagnetic core contribution and a paramagnetic contribution from the charge carriers. Europium substitution introduces localized magnetic moments into the lattice. Although direct exchange interaction between these moments is negligible due to the large Eu–Eu distances, the indirect interaction via the conduction electrons may induce a magnetically ordered ground state. Samples with x = 1 – 2 order ferromagnetically at temperatures below 5 K, with effective magnetic moments close to the free-ion value of Eu^{2+}. This is also confirmed by XAS measurements.

References

[1] *S. Paschen, W. Carrillo-Cabrera, M. Baenitz, V. H. Tran, A. Bentien, H. Borrmann, R. Cardoso Gil, R. Michalak, Y. Grin and F. Steglich*, in Development of the Institute and Scientific Report (Max Planck Institute for Chemical Physics of Solids, Dresden Germany, Nov. 2000)

[2] *S. Paschen, M. Baenitz, A. Bentien, W. Carrillo-Cabrera, F. M. Grosche, S. Kimura, V. Pacheco, U. Schwarz, J. Sichelschmidt, P. Simon, G. Sparn, P. Thalmeier, V. Voevodin, A. Yaresko, H. Q. Yuan, I. Zerec, Y. Grin and F. Steglich*, in Scientific Report 2001/2002 (Max Planck Institute for Chemical Physics of Solids, Dresden Germany, Jan. 2003)

[3] *H. Q. Yuan*, Superconductivity in Germanium clathrates and heavy-fermion systems. (Dissertation, TU-Dresden, Shaker Verlag, Aachen, 2003).

[4] *I. Zerec*, Electronic structure and tunneling states in clathrates (Dissertation, TU-Dresden, Shaker Verlag, Aachen, 2004).

[5] *A. Bentien*, Transport and magnetic properties of rare-earth containing clathrates and clathrate-like compounds (Dissertation, TU-Dresden, Shaker Verlag, Aachen, 2004).

[6] *A. M. Sanchez Lotero*, Thermal transport in strongly correlated electron systems (Dissertation, TU-Dresden, Shaker Verlag, Aachen, 2005).

[7] *W. Carrillo-Cabrera, H. Borrmann, S. Paschen, M. Baenitz, F. Steglich and Y. Grin*, J. Solid State Chem. **178** (2005) 715.

[8] *E. Zintl and G. Brauer*, Z. Phys. Chem. **B20** (1933) 245.

[9] *H. Schäfer*, Annu. Rev. Mater. Sci. **15** (1985) 1.

[10] *J. Sichelschmidt, V. Voevodin, S. Paschen, W. Carrillo-Cabrera, Y. Grin and F. Steglich*, Acta Phys. Polonica **34** (2002) 613.

[11] *I. Zerec, W. Carrillo-Cabrera, V. Voevodin, J. Sichelschmidt, F. Steglich, Y. Grin, A. Yaresko and S. Kimura*, Phys. Rev. B **72** (2005) 045122.

[12] *I. Zerec, A. Yaresko, P. Thalmeier and Y. Grin*, Phys. Rev. B **66** (2002) 045115.

[13] *H. Q. Yuan, F. M. Grosche, W. Carrillo-Cabrera, V. Pacheco, G. Sparn, M. Baenitz, U. Schwarz, Y. Grin and F. Steglich*, Phys. Rev. B **70** (2004) 174512.

[14] *J. Sichelschmidt, W. Carrillo-Cabrera, V. A. Ivanshin, Y. Grin and F. Steglich*, Eur. Phys. J. B **46** (2005) 201.

[15] *R. F. W. Herrmann, K. Tanigaki, T. Kawaguchi, S. Kuroshima and O. Zhou*, Phys. Rev. B **60** (1999) 13245.

[16] *W. Carrillo-Cabrera, J. Curda, K. Peters, S. Paschen, M. Baenitz, Y. Grin and H. G. von Schnering*, Z. Kristallogr. NCS **215** (2000) 321.

[17] *W. Carrillo-Cabrera, S. Budnyk, Y. Prots and Y. Grin*, Z. Anorg. Allg. Chem. **630** (2004) 2267.

[18] *R. Demchyna, U. Köhler, Y. Prots, W. Schnelle, M. Baenitz, U. Burkhardt, S. Paschen and U. Schwarz*, Z. Anorg. Allg. Chem. **632** (2006) 73.

[19] *U. Köhler, R. Demchyna, S. Paschen and U. Schwarz*, Physica B (2005 accepted)

[20] *V. Pacheco, A. Bentien, W. Carrillo-Cabrera, S. Paschen, F. Steglich and Y. Grin*, Phys. Rev. B **71** (2005) 165205.

[21] *S. Paschen, W. Carrillo-Cabrera, A. Bentien, V. H. Tran, M. Baenitz, Y. Grin and F. Steglich*, Phys. Rev. B **64** (2001) 214404.

[22] *G. S. Nolas, J. L. Cohn, G. A. Slack and S. B. Schujman*, Appl. Phys. Lett. **73** (1998) 178.

[23] *J. L. Cohn, G. S. Nolas, V. Fessatidis, T. H. Metcalf and G. A. Slack*, Phys. Rev. Lett. **82** (1999) 779.

[24] *V. Keppens, B. C. Sales, D. Mandrus, B. C. Chakoumakos and C. Laermans*, Philos. Mag. Lett. **80** (2000) 807.

[25] *A. Bentien, V. Pacheco, S. Paschen, Y. Grin and F. Steglich*, Phys. Rev. B **71** (2005) 165206.

[26] *I. Zerec and P. Thalmeier*, Physica B **359** (2005) 208.

[27] *I. Zerec, V. Keppens, M. A. McGuire, D. Mandrus, B. C. Sales and P. Thalmeier*, Phys. Rev. Lett. **92** (2004) 185502.

[28] *A. Migliori, J. L. Sarrao, W. M. Visscher, T. M. Bell, M. Lei, Z. Fisk and R. G. Leisure*, Physica B **183** (1993) 1.

[29] *B. C. Sales, B. C. Chakoumakos, R. Jin, J. R. Thompson and D. Mandrus*, Phys. Rev. B **63** (2001) 245113.

[30] *B. C. Chakoumakos, B. C. Sales and D. G. Mandrus*, J. Alloys Compd. **322** (2001) 127.

[31] *G. K. H. Madsen, K. Schwarz, P. Blaha and D. J. Singh*, Phys. Rev. B **68** (2003) 125212.

[32] *Y. Mudryk, P. Rogl, C. Paul, S. Berger, E. Bauer, G. Hilscher, C. Godart and H. Noël*, J Phys. Condens. Mat. **14** (2002) 7991.

[33] *P. Rogl, Y. Mudryk, C. Paul, S. Berger, E. Bauer, G. Hilscher, C. Godart and H. Noël*, in Book of abstracts, The 2nd Hiroshima Workshop on "Transport and thermal properties of Advanced Materials", 2002)

[34] *T. Kawaguchi, K. Tanigaki and M. Yasukawa*, Phys. Rev. Lett. **85** (2000) 3189.

[35] *V. Pacheco, W. Carrillo-Cabrera, V. H. Tran, S. Paschen and Y. Grin*, Phys. Rev. Lett. **87** (2001) 099601.

[36] *J. Dünner and A. Mewis*, Z. Anorg. Allg. Chem. **621** (1995) 191.

[37] *P. Varschni*, Phys. Rev. B **2** (1970) 3952.

---

[1] Present address: Kazan State University, Kazan, Russian Federation

[2] Present address: Vienna University of Technology, Vienna, Austria

[3] MPI for Physics of Complex Systems, Dresden, Germany

[4] University of Illinois at Urbana Champaign, Urbana, USA